

# Non-diffractive acoustic beams produce negative radiation force in certain regions

Cite as: AIP Advances **11**, 065029 (2021); <https://doi.org/10.1063/5.0056692>

Submitted: 13 May 2021 . Accepted: 03 June 2021 . Published Online: 18 June 2021

 Menyang Gong (宫门阳),  Yupei Qiao (乔玉配), Zhonghan Fei (费仲晗), Yuanyuan Li (李媛媛), Jiehui Liu (刘杰惠), Yiwei Mao (毛一蔚), Aijun He (何爱军), and  Xiaozhou Liu (刘晓宙)



View Online



Export Citation



CrossMark

## ARTICLES YOU MAY BE INTERESTED IN

[Far-field particle manipulation scheme based on X wave](#)

[Physics of Fluids](#) **32**, 117104 (2020); <https://doi.org/10.1063/5.0027525>

Call For Papers!

AIP Advances

SPECIAL TOPIC: Advances in  
Low Dimensional and 2D Materials



# Non-diffractive acoustic beams produce negative radiation force in certain regions

Cite as: AIP Advances 11, 065029 (2021); doi: 10.1063/5.0056692

Submitted: 13 May 2021 • Accepted: 3 June 2021 •

Published Online: 18 June 2021



View Online



Export Citation



CrossMark

Menyang Gong (宫门阳),<sup>1</sup> Yupei Qiao (乔玉配),<sup>1</sup> Zhonghan Fei (费仲晗),<sup>1</sup> Yuanyuan Li (李媛媛),<sup>1</sup> Jiehui Liu (刘杰惠),<sup>1</sup> Yiwei Mao (毛一蔚),<sup>1</sup> Aijun He (何爱军),<sup>2,a)</sup> and Xiaozhou Liu (刘晓宙)<sup>1,3,a)</sup>

## AFFILIATIONS

<sup>1</sup> Key Laboratory of Modern Acoustics, Institute of Acoustics and School of Physics, Collaborative Innovation Center of Advanced Microstructures, Nanjing University, Nanjing 210093, China

<sup>2</sup> School of Electronic Science and Engineering, Nanjing University, Nanjing 210023, China

<sup>3</sup> State Key Laboratory of Acoustics, Institute of Acoustics, Chinese Academy of Sciences, Beijing 100190, China

<sup>a)</sup> Authors to whom correspondence should be addressed: [haj@nju.edu.cn](mailto:haj@nju.edu.cn) and [xzliu@nju.edu.cn](mailto:xzliu@nju.edu.cn)

## ABSTRACT

A method of particle manipulation, one based on the force of acoustic radiation, has drawn wide attention. However, the real concept behind “acoustic tweezers”—negative acoustic radiation force (ARF)—has not been realized in experiments. In this paper, a prediction of a negative ARF generated by the non-diffractive acoustic beam is proposed. Its underlying physical mechanism is also analyzed in detail. On the basis of an analysis of energy flux density, the analytical region of negative radiation produced by the non-diffractive beam is solved completely. Forecast methods based on this solution are proposed that lay the foundation for realizing acoustic tweezers and offer the possibility of designing devices that produce negative ARFs. In addition, the negative propagation of acoustic beams in normal materials is realized, raising a possible alternative means to accomplish acoustic beam control.

© 2021 Author(s). All article content, except where otherwise noted, is licensed under a Creative Commons Attribution (CC BY) license (<http://creativecommons.org/licenses/by/4.0/>). <https://doi.org/10.1063/5.0056692>

## I. INTRODUCTION

After Wu proposed “acoustic tweezers” in 1991,<sup>1</sup> acoustic manipulation based on acoustic radiation force (ARF) has gradually become an attractive field of research. The near-field ARF of plane waves, Gaussian waves, and Bessel waves on regular particles, both spherical and cylindrical, has been widely studied.<sup>2–12</sup> A far-field ARF calculation scheme based on X beams has also been proposed.<sup>13</sup> In most acoustic nonlinear phenomena, the ARF appears as a thrust force. Only for a small number of circumstances have calculations of the ARF suggested a pulling force.

Being a non-intuitive phenomenon, the negative ARF has not been realized in experiments. In a large number of application scenarios, the control source can only be added in a small angular range relative to the controlled structure. Therefore, studying the negative ARF of a single beam is particularly important. To realize “acoustic tweezers” using only a single beam, determination of the area where particles may be subjected to a negative ARF is necessary. This prediction is usually complicated and difficult. Previously,

having calculated the ARF of spherical particles and spherical shells in non-viscous fluids, Marston explained the negative ARF generated through the notion of scattering suppression.<sup>7,8</sup> Azarpeyvand also proposed a structure that produces negative ARFs in the Bessel beam.<sup>14</sup>

In this paper, we provide a new method to find areas where particles may be subjected to a negative ARF. With our scheme, we believe that there is another mechanism that produces a negative ARF by a single wave beam on particles. The time average value of the output energy flow of the sound beam in the designated area is negative, which essentially constitutes a negative radiation area. In this negative radiation region, the ARF on particles is mostly negative.

Previous methods of analysis generally interpret the negative ARF as an asymmetry of scattering; that is, the acoustic field distribution of the controlled particles along the axial direction is asymmetric, and this asymmetry (radiation suppression<sup>7,8</sup>) brings about a negative ARF. Given that the non-diffractive beam solution has no strong selectivity of a particle structure,

it is considered to have a wide range of applications in particle manipulation.

## II. ANALYSIS OF ENERGY FLUX DENSITY OF ACOUSTIC BESSSEL BEAM

Using the cylindrical wave expansion, all acoustic non-diffractive beams can be expanded into a linear combination of different orders of Bessel beams. The completeness of the system of linear combinations for any non-diffractive beam permits us to choose acoustic Bessel beams for analysis. The output energy flux density  $S$  of a Bessel beam can be divided into two parts by mathematical arrangement—an axial component  $S_z$  and a rotational component  $S_\phi$ . The output behavior of the energy flux of the Bessel beam is determined by the complex amplitude of pressure and velocity potential. In cylindrical variables, both complex amplitudes take the form

$$\begin{aligned} p(\mathbf{r}, t) &= p(r, \phi) e^{i\beta z + im\phi - i\omega t}, \\ \Phi(\mathbf{r}, t) &= \Phi(r, \phi) e^{i\beta z + im\phi - i\omega t}, \end{aligned} \quad (1)$$

where  $p$  denotes the sound pressure,  $\Phi$  is the velocity potential,  $m$  is an integer number, and  $r$ ,  $z$ , and  $\phi$  are the three components of the cylindrical coordinate system; the parameters  $\beta$  and  $\omega$  are the longitudinal wave number and angular frequency, respectively. The sound pressure function and the components of the velocity potential function satisfy the Helmholtz equation. These functions satisfy Bessel's equation,<sup>15</sup>

$$\begin{aligned} \frac{d^2}{dr^2} p_z + \frac{m}{r} \frac{d}{dr} p_z + \left( q^2 - \frac{m^2}{r^2} \right) p_z &= 0, \\ \frac{d^2}{dr^2} \Phi_z + \frac{m}{r} \frac{d}{dr} \Phi_z + \left( q^2 - \frac{m^2}{r^2} \right) \Phi_z &= 0, \end{aligned} \quad (2)$$

where  $q$  denotes the transverse wave number; here,  $p_z$  and  $\Phi_z$  denote  $\partial p / \partial z$  and  $\partial \Phi / \partial z$ , respectively. For generality of expression, the complex amplitudes of the pressure and velocity potential can be written as

$$\begin{aligned} p_z &= a_1 J_m(qr), \\ \Phi_z &= a_2 J_m(qr), \end{aligned} \quad (3)$$

where  $a_1$  and  $a_2$  are amplitudes.

From the above arrangement, the pressure and velocity potential distributions of the acoustic Bessel beam depend on the parameters of the medium (density and compressibility) and the parameters of the incident wave, including the transverse wave number, the order of the acoustic Bessel wave number, the wave number in the medium, and amplitudes  $a_1$  and  $a_2$ .

Therefore, the energy flux density of the acoustic Bessel beam can be obtained by

$$\begin{aligned} \mathbf{S} = \frac{c}{8\pi} \left[ \frac{k\beta}{q^2} (|a_1|^2 + |a_2|^2) \left( J_m'^2 + \frac{m^2}{q^2 r^2} J_m^2 \right) \right. \\ \left. - \frac{2m}{q^3 r} (\beta^2 + k^2) \text{Im}(a_1 a_2^*) J_m' J_m \right] \mathbf{e}_z \\ + \frac{c}{8\pi} \left[ \frac{mk}{q^2 r} (|a_1|^2 + |a_2|^2) J_m^2 - \frac{2\beta}{q} \text{Im}(a_1 a_2^*) J_m' J_m \right] \mathbf{e}_\phi, \end{aligned} \quad (4)$$

where  $\beta^2 = k^2 - q^2$  and the prime on  $J_m(qr)$  denotes the derivative with respect to its argument  $qr$ . From Eq. (4), the energy flux density vector is found not to depend on the axial coordinate  $z$ , which confirms that the acoustic Bessel beam is non-diffractive. A corollary of the definition of the acoustic non-diffractive beam is that the vector structure of the energy flux density only contains an axial component and a rotational component, and hence the energy of the sound field does not leak (diffract) in the radial direction.

From their properties, the Bessel functions satisfy recurrence formulas,

$$\begin{aligned} J'_m &= \frac{1}{2} (J_{m-1} - J_{m+1}), \\ \frac{m J_m}{qr} &= \frac{1}{2} (J_{m-1} + J_{m+1}). \end{aligned} \quad (5)$$

From Eq. (5), the derivative term of the quantity in the energy flux density can be replaced by Bessel functions of  $m-1$  and  $m+1$  order,

$$\begin{aligned} \mathbf{S} = \frac{c}{8\pi} \left[ \frac{k\beta}{2q^2} (|a_1|^2 + |a_2|^2) (J_{m-1}^2 + J_{m+1}^2) \right. \\ \left. - \frac{\beta^2 + k^2}{2q^2} \text{Im}(a_1 a_2^*) (J_{m-1}^2 J_{m+1}^2) \right] \mathbf{e}_z \\ + \frac{cr}{32\pi m} \left[ k(|a_1|^2 + |a_2|^2) (J_{m-1} + J_{m+1})^2 \right. \\ \left. - 2\beta \text{Im}(a_1 a_2^*) (J_{m-1}^2 - J_{m+1}^2) \right] \mathbf{e}_\phi. \end{aligned} \quad (6)$$

From Eq. (6), the energy flux density decomposes into two terms: a radial component and a transverse component. For normal plane waves, both terms are positive, but when the distribution functions for both the velocity potential and sound pressure are out of phase (as for a non-diffractive beam), the term  $\text{Im}(a_1 a_2^*)$  may not vanish. In this instance, the behavior of this term can affect the sign of the whole component. After decomposition, both the axial  $S_z$  and rotational  $S_\phi$  components may have negative values. The region where  $S_z$  is negative defines the propagation region of negative acoustic radiation. Similarly, the region where  $S_z$  is positive defines the positive region of acoustic radiation propagation.

## III. NUMERICAL CALCULATION OF ENERGY FLUX DENSITY OF AN ACOUSTIC BESSSEL BEAM

To verify the inference derived from the formulas, numerical calculations were performed. Because most acoustic manipulation is conducted in liquid, the environmental medium selected here is water. For convenience in calculations, the modulus of both  $a_1$  and  $a_2$  is set to 1.

The radial distributions of the axial component of the energy flux density for Bessel beams of orders 1–4 (Fig. 1) were developed by fixing the transverse wave number and the phase difference between the complex amplitudes of sound pressure and velocity potential. For each Bessel beam of order  $m$ ,  $S_z$  of energy flux density can be negative. This means that the direction of flow of the acoustic energy in the negative region is opposite to that of the wave vector  $k$ . That is, the energy flows in the  $-z$  direction (in the direction of the sound source).

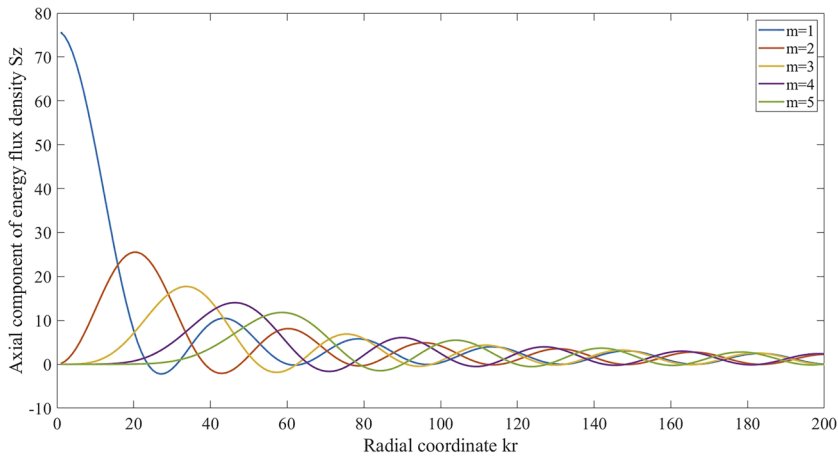


**FIG. 1.** Radial dependence of the axial component of the energy flux density of different orders. The phase difference is fixed at  $\pi/2$ . The transverse wave number is set at  $q = 0.9k$ . The different colored curves have different values of  $m$ , the order of the Bessel beam.

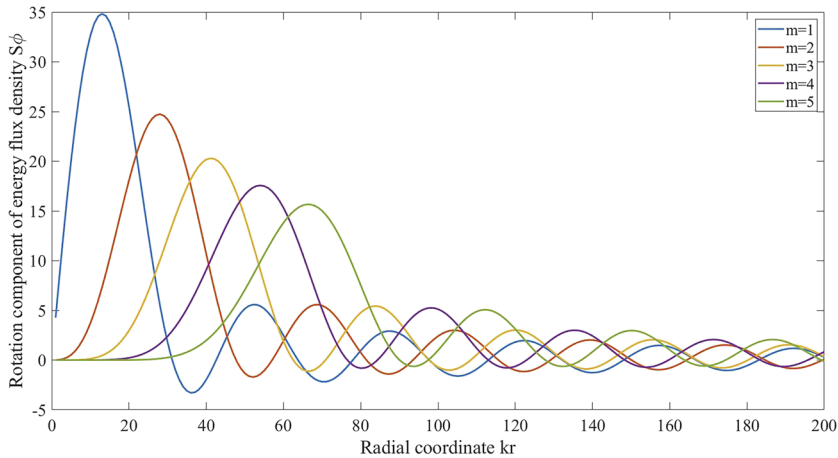


**FIG. 2.** Radial dependence of the rotation component of the energy flux density for different orders. The phase difference is fixed at  $\pi/2$ . The transverse wave number is set to  $q = 0.9k$ . The different colored curves have different Bessel orders  $m$ .

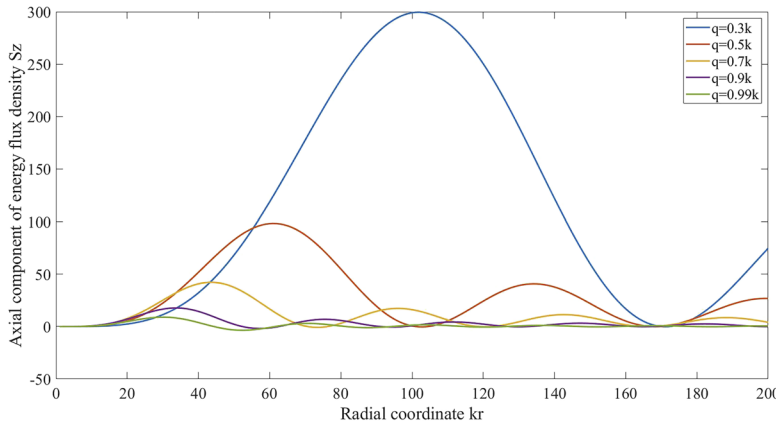


**FIG. 3.** Radial dependence of the axial component of energy flux density for different transverse wave numbers. The phase difference is fixed at  $\pi/2$ , and the order of the Bessel beam is fixed at  $m = 3$ . The different colored curves have different transverse wave numbers  $q$ .

Similarly, the radial distributions of the rotation component of the energy flux density for Bessel orders 1–4 were developed by fixing the transverse wave number and the phase difference between complex amplitudes of the sound pressure and velocity potential (Fig. 2). Component  $S_\phi$  of the energy flux density

for the Bessel beam alternates between positive and negative values, implying that the non-diffractive beam can transport angular momentum in two directions simultaneously in different regions.

The radial distributions of the axial component of the energy flux density of the third-order Bessel beam for various transverse

wave numbers (Fig. 3) were obtained by fixing the phase difference between the complex amplitudes of the sound pressure and velocity potential. From Fig. 3, when the transverse wave number is large (i.e.,  $q = 0.99k$ ), the intensity and width of the interval of negative acoustic energy transfer are more obvious.

The radial distributions of the rotation component of the energy flux density of the third-order Bessel beam for various transverse wave numbers (Fig. 4) were obtained by fixing the phase difference between the complex amplitudes of the sound pressure and velocity potential. From Fig. 4, where  $r$  is large, implying the argument of the Bessel function is large, the positive and negative intervals of the rotation components cross and gradually form a periodic structure. This periodicity arises from the far-field approximation of the Bessel function.

When the argument of the Bessel function is large (large  $r$  implies the region is far from the axis), the Bessel function can be written as

$$J_m(qr) = \sqrt{\frac{2}{\pi qr}} \cos\left(qr - \frac{\pi}{4} - \frac{m\pi}{2}\right). \quad (7)$$

By substituting Eq. (7) into Eq. (6), the far-field energy flux density approximates to

$$\mathbf{S} = \mathbf{S}_z + \mathbf{S}_\phi,$$

$$\mathbf{S}_z = \frac{ck\beta}{8\pi^2 q^3 r} (|a_1|^2 + |a_2|^2) [1 - (-1)^m \sin(2qr)] \mathbf{e}_z, \quad (8)$$

$$\mathbf{S}_\phi = -\frac{ck\beta}{8\pi^2 q^3 r} (-1)^{m+1} \frac{2q \operatorname{Im}(a_1 a_2^*)}{\beta} \cos(2qr) \mathbf{e}_\phi,$$

which shows that its axial component must be positive in the far field. Therefore, the region of negative sound propagation must appear near the axis. The rotational component is periodic and may also be positive or negative in the far field. The behavior of the rotational component of the Bessel beam with odd order differs by just  $\pi$  from that of the Bessel beam of even order.

Radial distributions of the axial component of the energy flux density for a first-order Bessel beam for various phase differences between the complex amplitudes of sound pressure and velocity potential (Fig. 5) were obtained by fixing the transverse wave

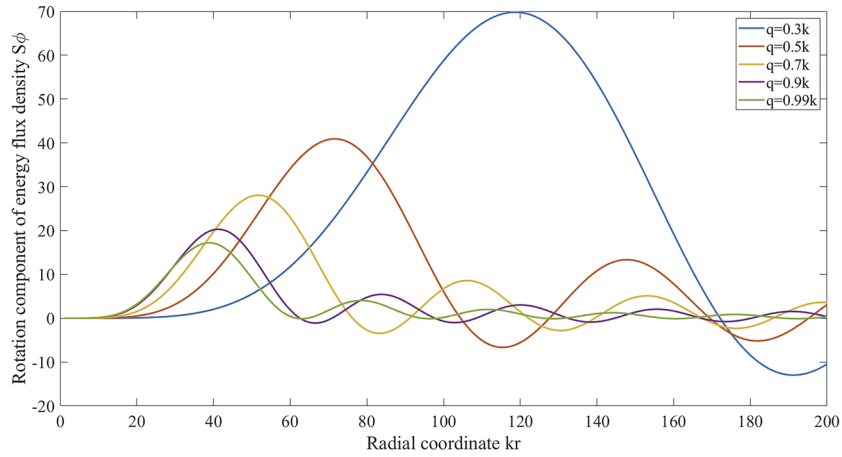


**FIG. 4.** Radial dependence of the rotation component of the energy flux density for different transverse wave numbers. The phase difference is fixed at  $\pi/2$ , and the Bessel order is fixed at  $m = 3$ . The different colored curves have different transverse wave number  $q$ .

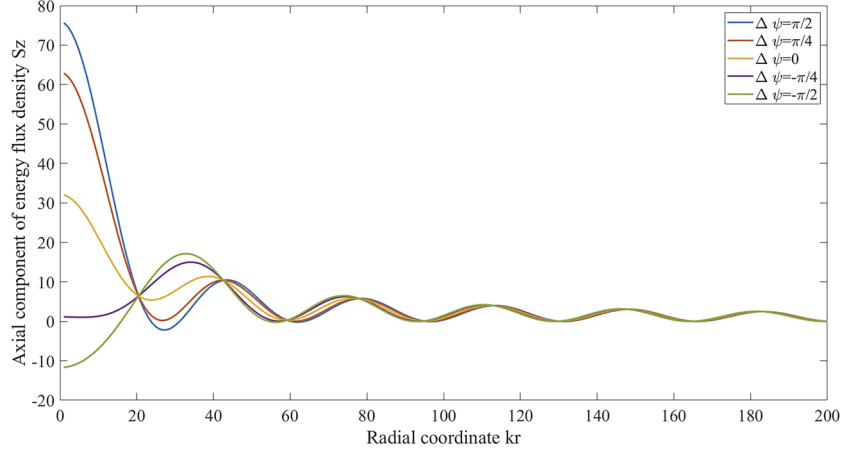


**FIG. 5.** Radial dependence of the axial component of the energy flux density for different phase differences. The transverse wave number is fixed at  $q = 0.9k$  and the Bessel order is  $m = 1$ . The different colored curves differ in  $\Delta\psi$ , the phase difference for the complex amplitudes of velocity potential and sound pressure.

number. From Fig. 5, when the phase difference is  $-\pi/2$ , an obvious negative sound propagation region arises in the paraxial region.

The radial distributions of the rotation component of the energy flux density of the first-order Bessel beam for various phase differences between the complex amplitudes of the sound pressure and velocity potential (Fig. 6) were obtained by fixing the transverse wave number. From Fig. 6, in the region for large  $r$  far from the axis, the rotation component shows periodicity consistent with the theory, as shown in Eq. (12).

From Figs. 3 and 5, a means of expanding the amplitude and region of negative axial energy flux density is evident:

- The larger the transverse wave number  $q$ , the wider the negative region of the axial component and the larger the amplitude. In other words, when the cone angle of the Bessel beam is larger, the negative value of the longitudinal component is larger.
- Another way to increase the negative amplitude of the axial component is to adjust the phase difference between the complex amplitudes of sound pressure and velocity potential. When  $r$  is small, which means when the selected area is near the axis,  $S_z$  may become negative. With  $\Delta\psi = -\pi/2$ , we

obtain the area with the largest negative value of this axial component.

From Figs. 4 and 6, a means to improve the amplitude and region of angular momentum transport capacity in two directions of the non-diffractive beam is possible:

- The smaller the transverse wave number  $q$ , the wider the negative region of the rotational component and the larger the amplitude. In other words, when the cone angle of the Bessel beam is larger, the amplitude of the rotation component is greater, and hence, the angular momentum transfer is stronger.
- When  $r$  is large, the curves for different phase differences tend to converge. In Fig. 6, there are two different types of curves because the two types of curves correspond to  $0 < \Delta\psi < -\pi$  and  $-\pi < \Delta\psi < 0$ . Bessel beams with the same parity in phase difference can be superimposed to enhance conveying capacity.

The behavior of the two components of the energy flux density of the 1–3 order Bessel beam (Figs. 7–9) was compared. From the analysis, each Bessel beam can be divided into three regions

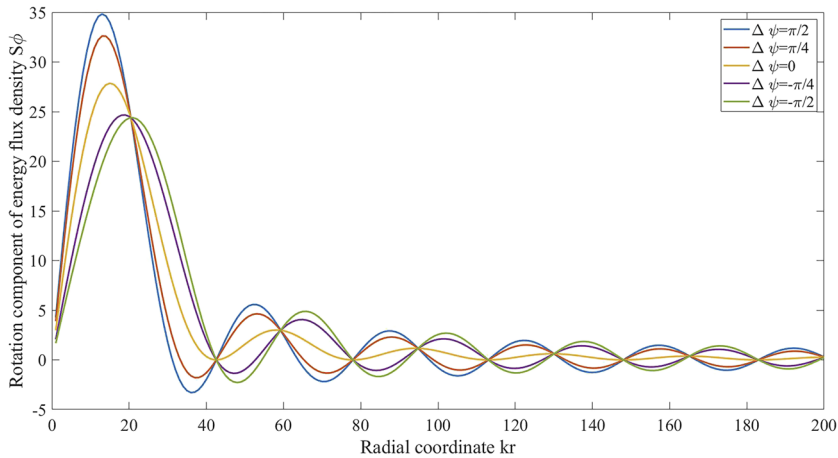


**FIG. 6.** Radial dependence of the rotation component of the energy flux density for various phase differences. The transverse wave number is set to  $q = 0.9k$ , and the Bessel order is set to  $m = 1$ . The different colored curves differ in  $\Delta\psi$ , the phase difference in the complex amplitudes of the velocity potential and sound pressure.

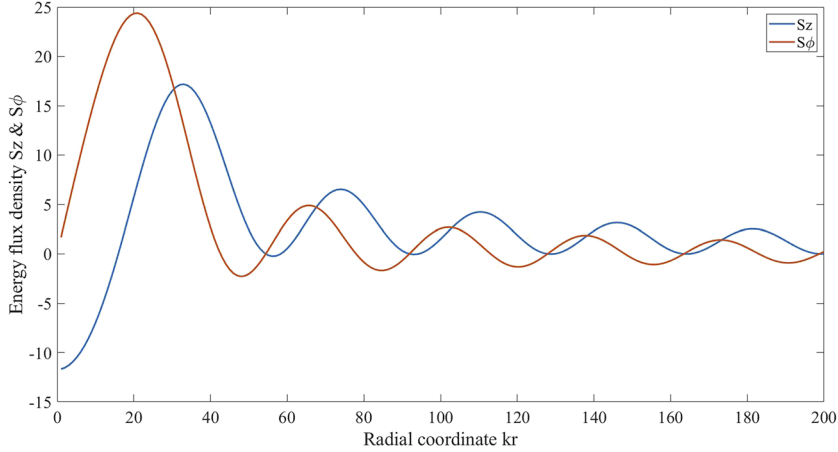


**FIG. 7.** Radial dependence of the two components of the energy flux density of the first-order acoustic Bessel beam ( $m = 1$ ). The phase difference is set to  $\pi/2$ , and the transverse wave number is set to  $q = 0.9k$ . The different colored curves represent the axial and rotation components of the energy flux density.

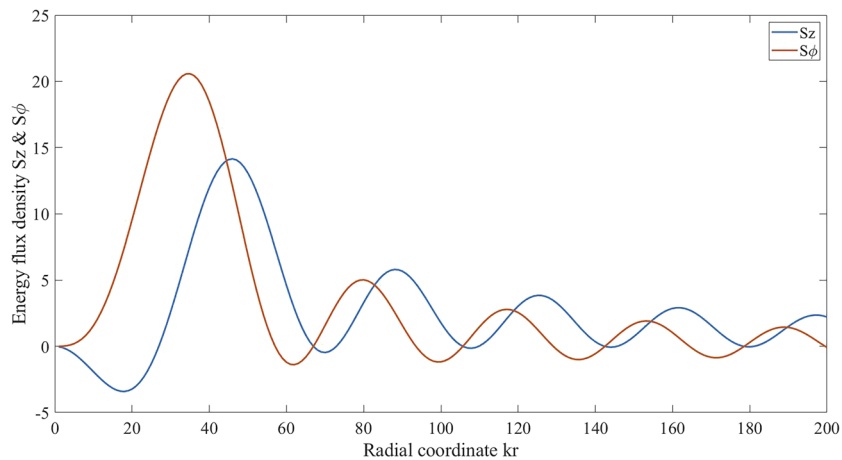


**FIG. 8.** Radial dependence of the two components of the energy flux density for the second-order acoustic Bessel beam ( $m = 2$ ). The remaining settings are as stated in Fig. 7.

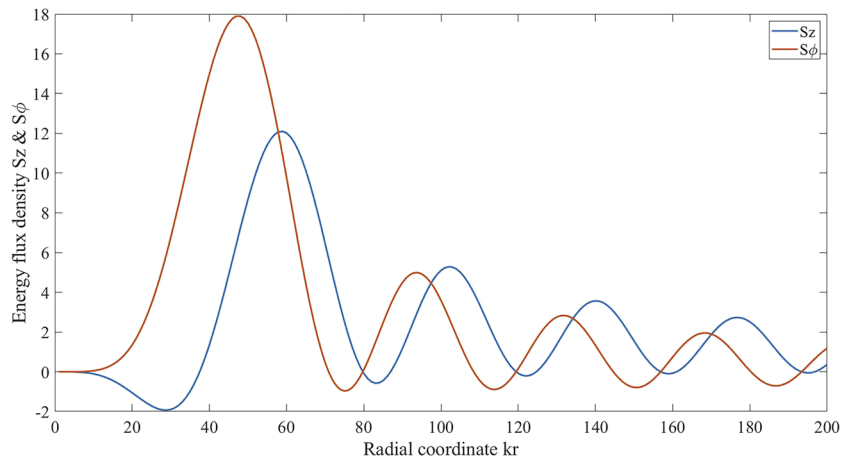


**FIG. 9.** Radial dependence of the two components of the energy flux density for the third-order acoustic Bessel beam ( $m = 3$ ). The remaining settings are as stated in Fig. 7.

according to their distance from the axis. Moreover, the parameter dependence of the components are different:

- When  $r$  is small, i.e., the region is close to the axis, the axial component of the energy flux density is negative, whereas the angular component is positive.
- Over a certain range of  $r$ , both components of the energy flux density are positive.
- When  $r$  is large, i.e., the region is far from the axis, the axial component of the energy flux density is positive, and alternating positive and negative values of the angular component appear.

The value can be used to determine regions in which to manipulate structures according to the different regional behavior of the two energy components. For example, in the paraxial region, particles can be given negative momentum, whereas in the region far from the axis, particles can obtain angular momentum in the opposite direction to the adjacent region.

In Figs. 10 and 11, the negative ARF area is illustrated vividly. The schematic (Fig. 10) shows that the negative ARF area is mainly distributed near the axis. Furthermore, in COMSOL simulations (Fig. 11), an obvious negative ARF region appears near the axis

region by fixing certain parameter settings (phase difference set to  $-\pi/2$ , transverse wave number  $q = 0.9k$ , and Bessel order  $m = 1$ ).

The axial component of the energy flux density is negative, signifying a negative ARF region in the acoustic wave. For the acoustic

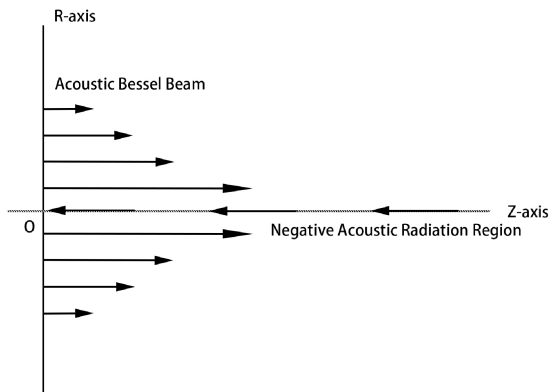


**FIG. 10.** Schematic of the negative propagation region of the non-diffractive sound beam.

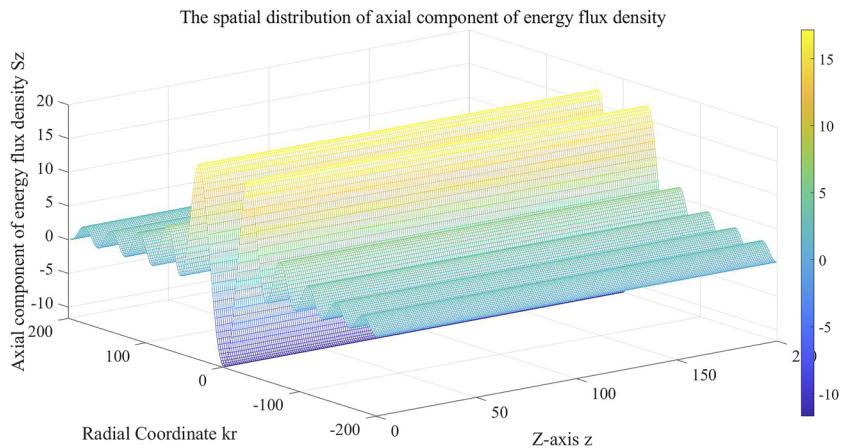


**FIG. 11.** Spatial distribution of the axial component of the energy flux density. The phase difference is fixed at  $-\pi/2$ , and the transverse wave number is set at  $q = 0.9k$ . The order of the Bessel beam is  $m = 1$ .

wave propagating in the forward energy flux density, the ARF acting on the structure is usually in the same direction as the wave vector,<sup>14</sup> that is, the same direction as the flow of the energy flux density. The created negative energy flux density region is equivalent to a reverse echo, for which the general structure in it usually receives a negative ARF. The distribution of the scattered sound pressure near the rigid spherical particles (Fig. 12) was plotted for the negative ARF region, which is defined as the constructed equivalent echo area, specifically, the area where the acoustic energy density flux is negative. Chromaticity, obtained from COMSOL calculations, represents the distribution of the scattered sound pressure in the area near the spherical particle, its radius being 1 mm. The scattered sound pressure on the side close to the sound source near the spherical particle (Fig. 12) is negative and that on the side away from the sound source is positive. From the sound pressure distribution, the particles are drawn toward the sound source by the negative ARF. In this way, acoustic tweezers may be constructed.

To illustrate further that this negative propagation area may be used to produce a negative ARF, we calculated the ARF acting on the spherical particles in this area,

$$\langle F \rangle = - \iint_{S(t)} \langle p \rangle \mathbf{n} d\mathbf{s}. \quad (9)$$

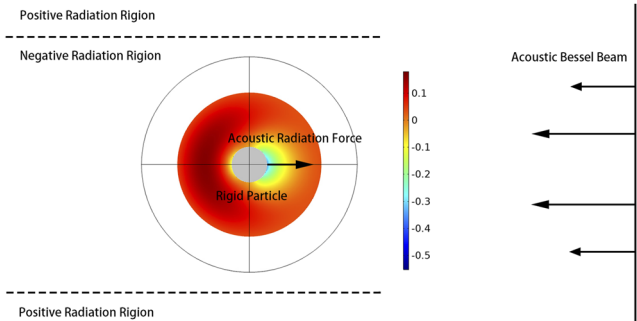


**FIG. 12.** Schematic of the sound pressure distribution near a spherical particle in the negative radiation region. Chromaticity, obtained using COMSOL, represents the distribution of the scattered sound pressure in the area near the spherical particle. The radius of the spherical particle is 1 mm.

The radius of the spherical particle ranged from 0.5 to 1.5 mm. The spherical particles for a set radius were all subjected to a negative ARF (Fig. 13). In contrast, the ARF acting on particles at 5 and 10 mm off-axis (Figs. 14 and 15, respectively), is positive, which also supports the idea that negative ARFs appear near the axis.

The behavior within the negative propagation region constructed by non-diffractive acoustic beams is similar to the physical behavior of negative refraction acoustic metamaterials, which has become an area of intense research recently. Metamaterials also support wave vectors and energy fluxes of opposite signs.

Here, we stress that the phenomenon of negative propagation of acoustic beams constructed by non-diffractive acoustic beams appears in traditional media with positive density and positive coefficients of elasticity. This discovery also has special significance for developments in acoustic beam control.

Furthermore, for negative regions of the energy flux density of the non-diffractive beam to appear near the axis, the value of the Bessel function is relatively small. When  $r$  is small, lower-order

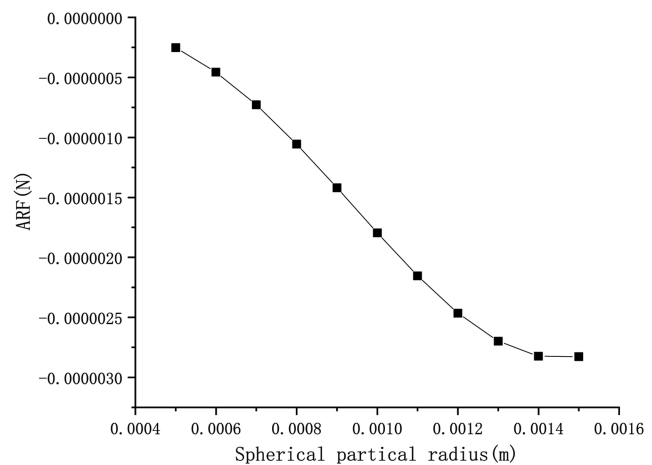


**FIG. 13.** ARFs on spherical particles in the negative propagation region (on-axis) of an acoustic Bessel beam. The radius of the spherical particle ranges from 0.5 to 1.5 mm.

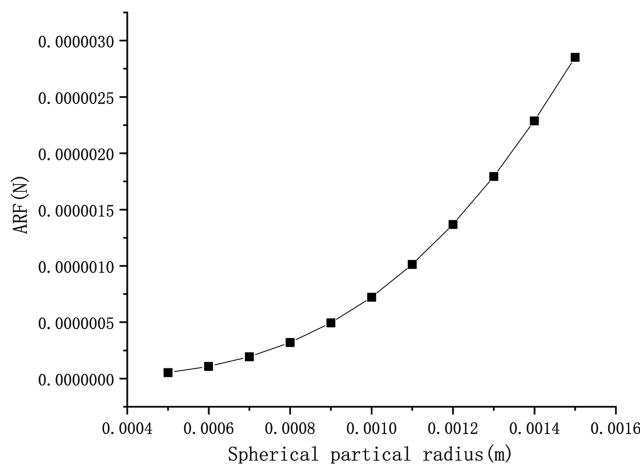


**FIG. 14.** ARFs on spherical particles in the positive propagation region of an acoustic Bessel beam. The distance between the particle center and the axis is 5 mm. The range in radius is as in Fig. 13.

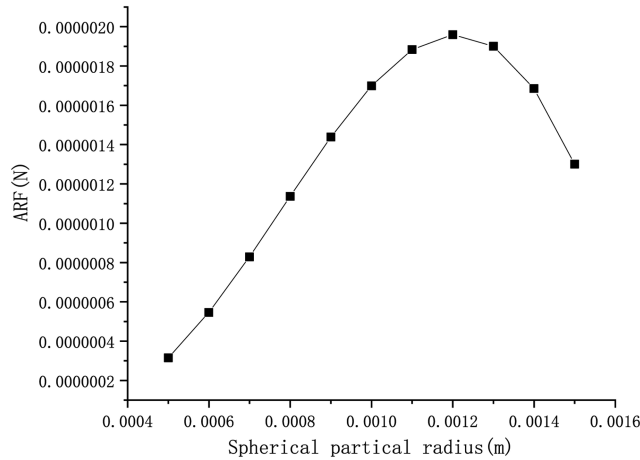


**FIG. 15.** ARFs on spherical particles in the positive propagation region of an acoustic Bessel beam. The distance between the particle center and the axis is 10 mm. The range in radius is as in Fig. 13.

Bessel functions are much larger than the higher-order Bessel functions  $J_m(kr) \gg J_{m+1}(kr)$ . Therefore, the axial component [Eq. (6)] can be further simplified using the paraxial approximation

$$\mathbf{S}_z = \frac{c}{16\pi q^2} [k\beta(|a_1|^2 + |a_2|^2) - (\beta^2 + k^2)\text{Im}(a_1 a_2^*)] J_{m-1}^2(qr) \mathbf{e}_z. \quad (10)$$

Moreover, the limiting condition of the phase difference in the negative ARF region of the energy flux density for non-diffractive beams yields

$$\begin{aligned} \pi + \arcsin(a) &< \Delta\psi < 2\pi - \arcsin(a), \\ a &= \frac{k\beta(|a_1|^2 + |a_2|^2)}{(\beta^2 + k^2)|a_1||a_2|}. \end{aligned} \quad (11)$$

For general media,  $a$  in Eq. (11) is always positive. This is the reason why non-diffractive acoustic beams near the axis have negative refraction.

This extraordinary conclusion does not violate the conservation of energy because the energy flux density  $S$  is calculated, not the energy flux  $P$  itself. If the energy flux density is integrated over an entire beam cross section, the energy flux is always positive from the expressions

$$\begin{aligned} \mathbf{P} &= \int_0^\infty \mathbf{S}(r) dr = \mathbf{P}_z + \mathbf{P}_\phi, \\ \mathbf{P}_z &= \frac{ck\beta}{8\pi q^2} (|a_1|^2 + |a_2|^2) \int_0^\infty J_{m-1}^2(r) dr \mathbf{e}_z > 0, \\ \mathbf{P}_\phi &= \frac{c}{8\pi} \left[ \frac{mk}{q^2} (|a_1|^2 + |a_2|^2) \int_0^\infty J_m^2(r) dr \right. \\ &\quad \left. - \frac{2\beta}{q} \text{Im}(a_1 a_2^*) \int_0^\infty J'_m J_m r dr \right] \mathbf{e}_\phi. \end{aligned} \quad (12)$$

However, the construction of a non-diffractive beam results in a region where sound energy propagates negatively. This negative transmission comes at a cost of positive transmission in other regions. For the whole region, the acoustic beam still exhibits positive propagation.

#### IV. DISCUSSIONS AND CONCLUSIONS

To summarize, negative ARFs can be produced by non-diffractive acoustic beams active in certain regions. The parameter ranges of these negative propagation regions were analyzed. The physical mechanism present in constructing negative ARFs by non-diffractive acoustic beams was explained in detail. With a reasonable near-field approximation, analytic conditions governing these parameter ranges were obtained which offer an analytical relation that helps in designing a negative radiation area. The negative region of the axial energy flux density, which can be used to exert a negative ARF on the structure in a sound field, was verified in numerical calculations. Alternating positive and negative regions of the rotating energy flux density over an entire sound field can exert an oppositely directed angular momentum. These two results are of great significance for further developments in acoustic manipulation of particles. An experimental verification of this theory is being performed. In addition, for non-diffractive beams, the negative propagation of an acoustic beam was realized in a normal material, opening a new area in acoustic beam control.

#### ACKNOWLEDGMENTS

This work was supported by the National Key R&D Program of China (Grant No. 2020YFA0211400); the State Key Program of National Natural Science of China (Grant No. 11834008); the National Natural Science Foundation of China (Grant No. 11774167); the State Key Laboratory of Acoustics, Chinese Academy of Sciences (Grant No. SKLA202008); the Key Laboratory of Underwater Acoustic Environment, Chinese Academy of Sciences (Grant

No. SSHJ-KFKT-1701); and the AQSIQ Technology R & D Program, China (Grant No. 2017QK125).

## DATA AVAILABILITY

The data that support the findings of this study are available from the corresponding author upon reasonable request.

## REFERENCES

- <sup>1</sup>J. Wu, "Acoustical tweezers," *J. Acoust. Soc. Am.* **89**, 2140–2143 (1991).
- <sup>2</sup>Z. Gong, P. L. Marston, and W. Li, "T-matrix evaluation of three-dimensional acoustic radiation forces on nonspherical objects in Bessel beams with arbitrary order and location," *Phys. Rev. E* **99**, 063004 (2019).
- <sup>3</sup>R. Wu, K. Cheng, X. Liu, J. Liu, Y. Mao, and X. Gong, "Acoustic radiation force on a double-layer microsphere by a Gaussian focused beam," *J. Appl. Phys.* **116**, 144903 (2014).
- <sup>4</sup>Y. Qiao, J. Shi, X. Zhang, and G. Zhang, "Acoustic radiation force on a rigid cylinder in an off-axis Gaussian beam near an impedance boundary," *Wave Motion* **83**, 111–120 (2018).
- <sup>5</sup>H. B. Wang, S. Gao, Y. P. Qiao, J. H. Liu, and X. Z. Liu, "Theoretical study of acoustic radiation force and torque on a pair of polymer cylindrical particles in two airy beams fields," *Phys. Fluids* **31**, 047103 (2019).
- <sup>6</sup>X. D. Fan and L. K. Zhang, "Trapping force of acoustical Bessel beams on a sphere and stable tractor beams," *Phys. Rev. Appl.* **11**, 014055 (2019).
- <sup>7</sup>P. L. Marston, "Negative axial radiation forces on solid spheres and shells in a Bessel beam (L)," *J. Acoust. Soc. Am.* **122**, 3162–3165 (2007).
- <sup>8</sup>P. L. Marston, "Axial radiation force of a Bessel beam on a sphere and direction reversal of the force," *J. Acoust. Soc. Am.* **120**, 3518–3524 (2006).
- <sup>9</sup>X. Zhang and G. Zhang, "Acoustic radiation force of a Gaussian beam incident on spherical particles in water," *Ultrasound Med. Biol.* **38**, 2007–2017 (2012).
- <sup>10</sup>S. Z. Hoque and A. K. Sen, "Interparticle acoustic radiation force between a pair of spherical particles in a liquid exposed to a standing bulk acoustic wave," *Phys. Fluids* **32**, 072004 (2020).
- <sup>11</sup>R. Wu, K. Cheng, X. Liu, J. Liu, X. Gong, and Y. Li, "Study of axial acoustic radiation force on a sphere in a Gaussian quasi-standing field," *Wave Motion* **62**, 63–74 (2016).
- <sup>12</sup>R. Wu, X. Liu, and X. Gong, "Axial acoustic radiation force on a sphere in Gaussian field," *Recent Dev. Nonlinear Acoust.* **1685**, 040010 (2015).
- <sup>13</sup>M. Gong, Y. Qiao, J. Lan, and X. Liu, "Far-field particle manipulation scheme based on X wave," *Phys. Fluids* **32**, 117104 (2020).
- <sup>14</sup>M. Azarpeyvand, "Prediction of negative radiation forces due to a Bessel beam," *J. Acoust. Soc. Am.* **136**, 547–555 (2014).
- <sup>15</sup>M. Abramowitz and I. A. Stegun, *Handbook of Mathematical Functions with Formulas, Graphs, and Mathematical Tables* (National Bureau of Standards, 1972).